Title

Corrigendum to “The triple argon isotope composition of groundwater on ten-thousand-year timescales” [Chemical Geology volume 583 (2021) 120458]

Authors

Seltzer, Alan M
Krantz, John A
Ng, Jessica
et al.

Publication Date

2022

DOI

10.1016/j.chemgeo.2021.120652

Peer reviewed

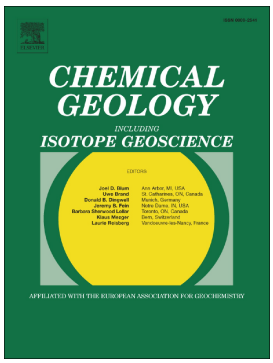

The triple argon isotope composition of groundwater on ten-thousand-year timescales

Alan M. Seltzer, John A. Krantz, Jessica Ng, Wesley R. Danskin, David V. Bekaert, Peter H. Barry, David L. Kimbrough, Justin T. Kulongoski, Jeffrey P. Severinghaus

PII: S0009-2541(21)00401-0

DOI: https://doi.org/10.1016/j.chemgeo.2021.120458

Reference: CHEMGE 120458

To appear in: *Chemical Geology*

Received date: 1 April 2021

Revised date: 16 July 2021

Accepted date: 23 July 2021

Please cite this article as: A.M. Seltzer, J.A. Krantz, J. Ng, et al., The triple argon isotope composition of groundwater on ten-thousand-year timescales, *Chemical Geology* (2018), https://doi.org/10.1016/j.chemgeo.2021.120458

The Triple Argon Isotope Composition of Groundwater on Ten-Thousand-Year Timescales

Alan M. Seltzer[1], John A. Krantz[1], Jessica Ng[2], Wesley R. Danskin[3], David V. Bekaert[1], Peter H. Barry[1], David L. Kimbrough[4], Justin T. Kulongoski[2,3], Jeffrey P. Severinghaus[2]

[1]Woods Hole Oceanographic Institution, Marine Chemistry & Geochemistry Department, Woods Hole, MA
[2]Scripps Institution of Oceanography, Geoscience Research Division, La Jolla, CA
[3]US Geological Survey, California Water Science Center, San Diego, CA
[4]San Diego State University, Geological Sciences, San Diego, CA

Abstract

Understanding the age and movement of groundwater is important for predicting the vulnerability of wells to contamination, constraining flow models that inform sustainable groundwater management, and interpreting geochemical signals that reflect past climate. Due to both the ubiquity of groundwater with order ten-thousand-year residence times and its importance for climate reconstruction of the last glacial period, there is a strong need for improving geochemical dating tools on this timescale. Whereas ^{14}C of dissolved inorganic carbon and dissolved ^{4}He are common age tracers for Late Pleistocene groundwater, each is limited by systematic uncertainties related to aquifer composition and lithology, and the extent of water-rock interaction. In principle, radiogenic ^{40}Ar in groundwater acquired from decay of ^{40}K in aquifer minerals should be insensitive to some processes that impact ^{14}C and ^{4}He and thus represent a useful, complementary age tracer. In practice, however, detection of significant radiogenic ^{40}Ar signals in groundwater has been limited to small number of studies of extremely old groundwater (>100 ka). Here we present the first high-precision (<1‰) measurements of triple Ar isotopes (^{40}Ar, ^{38}Ar, ^{36}Ar) in groundwater. We introduce a model that distinguishes radiogenic ^{40}Ar from atmospheric ^{40}Ar by using the non-radiogenic Ar isotopes (^{36}Ar, ^{38}Ar) to correct for mass-dependent fractionation. Using this model, we investigate variability in radiogenic ^{40}Ar excess ($\Delta^{40}Ar$) across 58 groundwater samples collected from 36 wells throughout California (USA). We find that $\Delta^{40}Ar$ ranges from ~0‰ (the expected minimum value) to +4.2‰ across three study areas near Fresno, San Diego, and the western Mojave Desert. Based on measurements from a network of 23 scientific monitoring wells in San Diego, we find evidence for a strong dependence of $\Delta^{40}Ar$ on aquifer lithology. We suggest that $\Delta^{40}Ar$ is fundamentally controlled by the weathering of old K-bearing minerals and thus reflects both the degree of groundwater-rock interaction, which is related to groundwater age, and the integrated flow through different geological formations. Future studies of Late Pleistocene groundwater may benefit from high-precision triple Ar isotope measurements as a new tool to better interpret ^{14}C- and ^{4}He-based constraints on groundwater age and flow.

1. Introduction

The abundance and isotopic composition of noble gases in groundwater are governed by inputs from the atmosphere and solid Earth, and by subsequent modification due to physical processes. As noble gases are chemically and biologically inert, they are sensitive only to physical fractionation mechanisms. Despite this apparent simplicity, our understanding of noble gases in groundwater continues to evolve as new groundwater systems are studied and new levels of analytical precision are achieved. For decades, it has been widely recognized that the dissolved noble gas content of recently recharged groundwater is set primarily by temperature-dependent diffusive equilibration with atmosphere-derived soil air (e.g. Mazor, 1972; Andrews and Lee, 1979), and secondarily by the dissolution of entrapped soil air bubbles leading to "excess air" (e.g. Aeschbach-Hertig et al., 2000; Heaton and Vogel, 1981; Stute et al., 1995). Once isolated from soil air, groundwater progressively "ages" in an aquifer (e.eg. Andrews and Lee, 1979; Bethke and Johnson, 2008; Suckow, 2014) and can acquire additional inert gases from crustal or mantle sources (e.g., Ballentine and Burnard, 2002; Deeds et al., 2008; Kulongoski et al., 2005). The isotopic composition and abundance of groundwater helium are particularly sensitive to non-atmospheric sources of noble gases, owing to the low solubility, and thus, small atmosphere-derived component of helium in groundwater (e.g., Kulongoski and Hilton, 2012). In particular, the radiogenic ^{4}He content of groundwater—derived from alpha decay of U and Th, which are both ubiquitous in crustal aquifer minerals—has been widely used as a groundwater dating tool on ten-thousand-year timescales (e.g., Andrews and Lee, 1979; Solomon et al., 1996), especially where complications associated with dissolved inorganic carbon (DIC) chemistry prohibit the direct application of ^{14}C as an age tracer (e.g., Aeschbach-Hertig et al., 2002; Clark et al., 1997). However, the relationship between groundwater residence

time and radiogenic ^{4}He is complex, requiring consideration of (i) the U/Th content, chemical weatherability, and age of aquifer minerals; (ii) fault enhancement of He transport; and the (iii) susceptibility of various minerals to diffusive helium loss to groundwater (Kulongoski et al., 2005; Solomon et al., 1996; Stute et al., 1992; Torgersen and Clarke, 1985).

Another radiogenic noble gas isotope that offers promise as a hydrogeological tracer in groundwater is ^{40}Ar, which is produced in aquifer minerals via the electron capture decay pathway of ^{40}K (McDougall and Harrison, 1999). However, because ^{40}Ar is three orders of magnitude more abundant than helium in the atmosphere (COESA, 1976) and roughly four times more soluble (Jenkins et al., 2019), radiogenic ^{40}Ar signals in groundwater are often dwarfed by background atmospheric ^{40}Ar. Consequently, few previous studies have detected radiogenic ^{40}Ar signals in groundwater (Andrews et al., 1989; Lippmann et al., 2003; Andrews et al., 1991; Torgersen et al., 1989). For clarity, we refer to a radiogenic ^{40}Ar signal as a measured ^{40}Ar/^{36}Ar ratio above the atmospheric value accompanied by an atmosphere-like ratio of the two stable non-radiogenic isotopes of Ar (^{38}Ar and ^{36}Ar). For example, roughly 1-10% anomalies of ^{40}Ar/^{36}Ar relative to the atmosphere have been detected in order 100 ka groundwater in Australia (Torgersen et al., 1989), in methane-rich shale-confined groundwater in Canada (Andrews et al., 1991), as well as in mixtures between relatively young (orders 1 to 10 ka) groundwaters and much older (>1 Ma) brines in Scandinavia (Andrews et al., 1989). In a deep South African system, ^{40}Ar/^{36}Ar ratios ~3 to 30 times the atmospheric value were observed in roughly 1-100 Ma groundwater (Lippmann et al., 2003). The highest dissolved ^{40}Ar/^{36}Ar ratios ever reported, over 100 times the atmospheric value, were measured in up to 2.64 Ga fracture fluids in the Canadian Shield (Holland et al., 2013). Notably, however, in order 100-ka groundwater samples from the Guarani aquifer in South America that were precisely dated with ^{81}Kr (Aggarwal et al.,

2015), all measured $^{40}Ar/^{36}Ar$ ratios were found to be equal to the atmospheric value within order 0.1% analytical uncertainties.

Given the wide range of radiogenic $^{40}Ar/^{36}Ar$ anomalies measured in old groundwaters, it remains unclear whether radiogenic argon isotope signals (below the analytical precision of conventional static mass spectrometry, ~1‰) exist in younger groundwaters. A further complication at the 1‰ level and below is that physical isotopic fractionation of atmosphere-derived argon due to soil air processes (Seltzer et al., 2019b; Seltzer et al., 2017; Severinghaus et al., 1996) and isotopic solubility differences (Seltzer et al., 2019a) must be taken into account to isolate radiogenic signals. A related example is high-precision measurement of argon isotopes in occluded air bubbles in glacial ice (0.01‰; Severinghaus et al., 2003). Studies of ice-core Ar isotopes over the last two decades have successfully separated radiogenic from physical signals of fractionation by measuring all three stable Ar isotopes at high precision (0.005‰; Bender et al., 2008; Higgins et al., 2015; Yan et al., 2019). A similar approach is needed to resolve radiogenic ^{40}Ar anomalies in groundwater at the 1‰ level or lower.

Given the prevalence of order ten-thousand-year old groundwater throughout aquifers worldwide (Befus et al., 2017), its important role as a source of drinking water (Gleeson et al., 2016; Jasechko et al., 2017), and its value for paleoclimatic reconstruction of the last glacial period (e.g., Aeschbach-Hertig and Solomon, 2013; Seltzer et al., 2021), there is a strong need for additional tracers to complement existing geochemical tools (i.e., ^{14}C and ^{4}He) used on this timescale, and to better constrain groundwater residence times and flow models. Recent advances in analytical techniques have permitted order 0.01‰ precision measurements of dissolved noble gas isotope ratios in groundwater (Seltzer et al., 2019a), as well as a more comprehensive view of the physical fractionation mechanisms in soil air (Seltzer et al., 2019b;

Seltzer et al., 2017) and the isotopic solubility and diffusivity differences in water (Bourg and Sposito, 2008; Seltzer et al., 2019a; Tempest and Emerson, 2013; Tyroller et al., 2018, 2014). Consequently, the conceptual and analytical basis for investigating Ar isotopes in younger groundwater is now well established. In this study, we present Ar isotope data from 58 groundwater samples collected from 36 wells throughout California groundwater systems, along with ^{3}H, ^{14}C of DIC, alongside major, minor, and trace element chemistry previously measured and reported by the United States Geological Survey. Using these data, we explore the potential for high-precision triple argon isotope measurements as a new hydrogeological indicator on ten-thousand-year timescales.

2. The Expected Triple Argon Isotope Composition of Groundwater

In this study, we assume that the ^{40}Ar content of groundwater is derived from two sources: the atmosphere and radioactive decay of ^{40}K in aquifer minerals. We neglect any potential mantle sources of Ar, given that mantle He sources have been demonstrated to be rather small, even in the western Mojave Desert regional aquifer, which is the nearest of our study areas to the San Andreas Fault and contains groundwater previously shown to have up to 6% mantle-derived helium (Kulongoski et al., 2003). As an illustrative example, because Ar is ~4 times more soluble than He (Jenkins et al., 2019) and ~1800 times more abundant in the atmosphere (COESA, 1976), assuming the $^{4}He/^{40}Ar$ ratio of the upper mantle is ~2 (Marty and Zimmermann, 1999) and the $^{3}He/^{4}He$ ratio is ~8 times larger than the atmospheric ratio (Sarda and Graham, 1990), the maximum observed mantle-derived ^{3}He fraction in Mojave Desert groundwater of ~6% (Kulongoski et al., 2003) translates to a ^{40}Ar excess (relative to air-saturated water) of 0.00001% (0.0001‰ or 0.1 per meg). Since this value is two orders of magnitude below our

analytical precision, we can dismiss mantle derived Ar as a significant contribution to the measured Ar isotopic ratio.

We define δ values with respect to the modern atmosphere (in ‰), such that:

$$\delta^{H}/_{L}Ar \equiv ({}^{H}Ar/{}^{L}Ar)_{meas}/({}^{H}Ar/{}^{L}Ar)_{atm} - 1 \qquad (1)$$

where the superscripts *H* and *L* refer to heavy and light isotope masses, respectively, and the subscripts *meas* and *atm* refer to measured and atmospheric ratios, respectively. We then define excess radiogenic ^{40}Ar ($\Delta^{40}Ar$) in groundwater using the ratio of radiogenic ^{40}Ar ($^{40}Ar_{rad}$) to atmosphere-derived ^{40}Ar ($^{40}Ar_{atm\text{-}d}$). Similar to Bender et al. (2008), we posit that all physical fractionation of atmosphere-derived $^{40}Ar/^{36}Ar$ is linearly proportional to physical fractionation of $^{38}Ar/^{36}Ar$, with respect to modern atmospheric air. In other words, we define $\Delta^{40}Ar$ (in ‰) as:

$$\Delta^{40}Ar \equiv {}^{40}Ar_{rad}/{}^{40}Ar_{atm\text{-}d} = \delta^{40}/_{36}Ar_{meas} - a \times \delta^{38}/_{36}Ar_{meas} + b \qquad (2)$$

where $\delta^{40}/_{36}Ar_{meas}$ and $\delta^{38}/_{36}Ar_{meas}$ refer to relative differences between measured and modern atmospheric ratios of $^{40}Ar/^{36}Ar$ and $^{38}Ar/^{36}Ar$ (Eq. 1), respectively, and *a* and *b* refer to the regression coefficients of a linear fit between $\delta^{40}/_{36}Ar$ and $\delta^{38}/_{36}Ar$ simulated by a physical fractionation model.

To estimate *a* and *b*, we used the coupled soil air/dissolution/excess air model presented in Seltzer et al. (2019b) to carry out simulations over a wide range of plausible combinations of water table depth, surface air humidity, geothermal gradient, recharge temperature, and excess air parameters. Briefly, our model considers physical isotopic fractionation of atmosphere-derived Ar that occurs due to steady-state diffusive processes in soil air as well as isotopic solubility differences and associated sensitivity to excess air input. In soil air, we assume that heavy Ar isotopes are enriched relative to lighter isotopes by gravitational settling (Schwander, 1989), but depleted due to the ternary effect of steady-state diffusion of atmospheric Ar into the

unsaturated zone (UZ) against an upward flux of water vapor (Seltzer et al., 2017; Severinghaus et al., 1996). In addition, thermal diffusion acts to favor the lighter isotopes with depth due to the geothermal gradient (Grachev and Severinghaus, 2003). At the water table, we model the preferential dissolution of heavy Ar isotopes using their well-constrained isotopic solubility differences (Seltzer et al., 2019a), and account for entrapment and partial dissolution of soil air bubbles using the Closed-system Equilibrium (CE) model (Aeschbach-Hertig et al., 2000). Our model considers combinations (n=4800) of plausible water table depths between 0 and 120 m, geothermal gradients between 0 and 0.06 K m^{-1}, surface atmospheric water vapor mole fractions between 0 and 2%, water table temperatures between 10 and 25°C, and entrapped air and fractionation parameters (*A* and *F* in the CE model) from 0 to 0.05 cm^3_{STP} g^{-1} and 0 to 1, respectively.

Modeled deviations of groundwater Ar isotope ratios ($\delta^{40}/_{36}Ar$ and $\delta^{38}/_{36}Ar$) with respect to the modern atmosphere are shown in Figure 1. As expected, there is a strong linear relationship between simulated $\delta^{40}/_{36}Ar$ and $\delta^{38}/_{36}Ar$ (R^2 = 0.9996) such that a = 1.9918 and b = -0.02‰ in equation 1. Whereas we expect an exact mass proportionality for gravitational fractionation (which is generally the leading fractionation mechanism in soil air; Seltzer et al., 2017), slight departures from ~2:1 fractionation of $\delta^{40}/_{36}Ar$ and $\delta^{38}/_{36}Ar$ are expected for thermal diffusion, water-vapor flux fractionation, and solubility fractionation (Seltzer et al., 2017; Seltzer et al., 2019a), the latter of which primarily gives rise to the slightly negative, non-zero b value. Residual values of $\delta^{40}/_{36}Ar$ from the linear regression (Figure 1 inset) are small, with a 95% confidence range between -0.027 and +0.025‰. Combining these model residuals with the measurement uncertainties for $\delta^{40}/_{36}Ar$ and $\delta^{38}/_{36}Ar$, we conservatively suggest a total ±2σ uncertainty of 0.1‰ for $\Delta^{40}Ar$. To avoid potential confusion, we emphasize that while $\Delta^{40}Ar$ is

expected to be positive in groundwater samples containing $^{40}Ar_{rad}$, the similar definition of $\Delta^{40}Ar$ for studies of ice core air bubbles (Bender et al., 2008) makes use of the concept that $\Delta^{40}Ar$ will be negative in samples of ancient air because the atmosphere is gradually accumulating radiogenic ^{40}Ar that is degassing from the solid Earth. Since the rate of ^{40}Ar accumulation in the atmosphere is ~0.066‰ Ma^{-1} (Bender et al., 2008), the total bias introduced in our definition of $\Delta^{40}Ar$ by assuming no atmospheric change over time is only ~0.007‰ for 100 ka groundwater, which is well below our analytical precision. Thus, over the ten-thousand-year timescale considered in this study, we neglect paleo-atmospheric changes in ^{40}Ar in our definition of $\Delta^{40}Ar$ (i.e., equation 2).

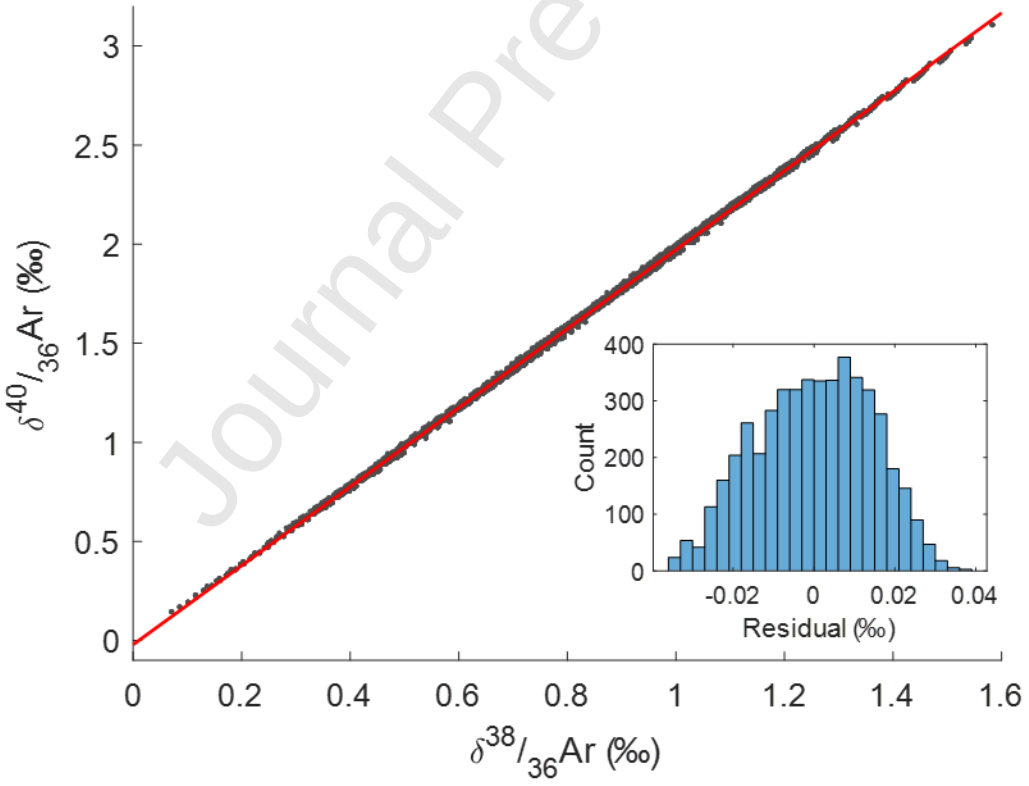

Figure 1: Simulated deviations of atmosphere-derived groundwater Ar isotopes ($\delta^{40}/_{36}Ar$ and $\delta^{38}/_{36}Ar$) with respect to the modern atmosphere, for 4800 combinations (grey dots) of water table depth, geothermal gradient, surface air humidity, water table temperature, and excess air parameters. The linear regression (red line) yields coefficients a=1.9918 and b=-0.02‰ in equation 2, with correlation coefficient r=0.9998. The distribution of simulated $\delta^{40}/_{36}Ar$ residuals from the linear fit is shown in the inset and has a 95% confidence range between -0.027 and +0.025‰.

3. Groundwater sampling and analysis

This study is focused on the stable isotopic composition of dissolved Ar in groundwater samples that were collected in evacuated 2-L glass flasks, quantitatively degassed by helium sparging, and analyzed via dynamic dual-inlet isotope ratio mass spectrometry (IRMS) in 2018 in the Noble Gas Isotope Laboratory at Scripps Institution of Oceanography (SIO; Seltzer et al., 2019a). This new analytical technique differs from traditional static noble gas measurements of copper tube samples and is described in detail in Seltzer et al. (2019a). Briefly, the technique achieves two orders-of-magnitude higher precision than conventional copper tube samples (e.g., Beyerle et al., 2000) by collecting, processing, and then analyzing large purified noble gas aliquots (~0.5-1.0 mL_{STP} of Ar, and roughly air-equilibrated noble gas ratios) on a Thermo-Finnigan MAT253 IRMS. The use of large gas samples eliminates the need for a carrier gas, as the total gas pressure in the IRMS bellows can be maintained at ~40 mbar throughout an ~8-hour analysis by compression of the bellows. Before analysis, 2-L samples are first degassed by sparging for 90 minutes with gaseous helium at 1 atm. Then, extracted gases are collected on a flow-through stainless-steel dip tube immersed in a 4-K liquid helium dewar, before being purified by gettering with Ti sponge and SAES Zr/Al sheets at 900 ºC, which removes all reactive gases. Next, pure noble gas aliquots are cryogenically transferred into another stainless-steel dip tube immersed in liquid helium. After three hours of equilibration in the dip tube at room temperature, noble gases are introduced to the MAT253 inlet and analyzed against an internal reference gas. Air samples collected from the SIO pier are routinely analyzed against the same internal reference gas, and all final groundwater data are thus reported as deviations from the well-mixed atmosphere, based on the mean of all air standard analyses. We refer the reader to Seltzer et al. (2019a) for additional details.

The original purpose of these groundwater measurements was to investigate gravitational settling signals recorded by the isotopic composition of dissolved Kr and Xe as a tracer of past water table depth (Seltzer et al., 2019b). In addition to Kr and Xe isotope measurements and dissolved Ar, Kr, and Xe concentrations, $^{40}Ar/^{36}Ar$ and $^{38}Ar/^{36}Ar$ ratios were also measured at ~0.02‰ precision (±1σ) in the same extracted dissolved gas aliquots. However, these Ar isotope data were not included in Seltzer et al. (2019b) because Ar isotopes are less sensitive to gravitational settling relative to non-gravitational sources of fractionation in soil air (Seltzer et al., 2017) and equilibrium solubility isotope effects (Seltzer et al., 2019a). Additionally, ^{40}Ar is affected by radioactive decay of ^{40}K in aquifer minerals whereas Kr and Xe lack any appreciable radiogenic sources in sedimentary aquifers over ten-thousand-year timescales, rendering Ar isotopes more difficult to interpret in the context of gravitational setting signals. These Ar isotope measurements thus provide a unique opportunity to investigate and distinguish signals of physical fractionation of atmosphere-derived Ar and radiogenic ^{40}Ar accumulation in groundwater. To demonstrate the reproducibility of these measurements, in Supplementary Figure S2 we show a histogram of replicate groundwater $\Delta^{40}Ar$ anomalies (from the mean of all replicates, typically two per well).

Groundwater samples were collected from supply and monitoring wells in three sedimentary groundwater systems: unconfined aquifers near Fresno, California and in the western Mojave Desert, and both a confined regional aquifer and unconfined local groundwater system in San Diego, California. In total, five samples from two wells were collected from Fresno, 18 samples from 11 wells were collected from the western Mojave Desert, and 35 samples from 23 scientific monitoring wells across six sites with multiple wells accessing different depth intervals were collected from San Diego. All samples were collected after

flushing three casing volumes from each well. For additional important context in interpreting these Ar isotope data, we include previous measurements of other key geochemical parameters in samples collected from each of these 36 wells by the USGS, following standard USGS groundwater sampling protocols (Arnold et al., 2018, 2016). For these additional data, the carbon isotopic composition of DIC was analyzed at the Woods Hole Oceanographic Institution National Ocean Sciences Accelerator Mass Spectrometry lab (Roberts et al., 2010); major and trace elements were measured via ICPMS/AES, AAS, and ion chromatography at the USGS National Water Quality lab (Fishman, 1993; Garbarino et al., 2006); water isotopes at the USGS Reston Stable Isotope Lab (Revesz et al., 2009); tritium at the USGS Menlo Park Tritium Lab (Oestlund and Dorsey, 1977); and noble gas abundances (for the Mojave Desert samples only) at USGS Denver Noble Gas Laboratory (Hunt, 2015).

4. Results and Discussion

4.1. Inter-aquifer Trends and Variability in $\Delta^{40}Ar$

Across all groundwater samples analyzed in this study, observed $\delta^{40}/_{36}Ar$ values vary between 0.81‰ and 6.26‰, while $\delta^{38}/_{36}Ar$ values vary between 0.41‰ and 1.67‰ (Figure 2). In total, 30 of 58 samples (from 21 of 36 wells) plot within error of the simulated line of best fit for physical fractionation of atmosphere-derived argon (i.e, $|\Delta^{40}Ar| < 0.1‰$), including all samples that predominantly reflect recharge over the past several decades [i.e., samples with tritium activities above 0.5 tritium units (TU)]. We observe a maximum $\Delta^{40}Ar$ value of 4.27 ± 0.10‰ (2σ) and a minimum of -0.11‰ ± 0.10‰ (2σ). In Figure 3, we find that samples with ^{14}C activities of DIC greater than 50 percent modern carbon (pmC) have zero $\Delta^{40}Ar$, within error. Our finding that virtually all samples have positive $\Delta^{40}Ar$ – including those dominated by recent

(<5 ka) recharge, as indicated by high ^{14}C and/or ^{3}H activities – suggests that our implementation of equation 2 successfully separates radiogenic sources of ^{40}Ar from the atmosphere-derived pool of ^{40}Ar. We note that one could use $\Delta^{40}Ar$ to determine the concentration of $^{40}Ar_{rad}$ ($[^{40}Ar_{rad}]$) using the following conversion:

$$[^{40}Ar_{rad}] = \frac{[^{40}Ar]}{1+1/\Delta^{40}Ar} \qquad (3)$$

Because total ^{40}Ar concentrations ($[^{40}Ar]$) are quite similar for all samples analyzed in this study (with a mean of (3.6 ± 0.28) x 10^{-4} cm^3_{STP} g^{-1}), $^{40}Ar_{rad}$ and $\Delta^{40}Ar$ are extremely well correlated (R^2=0.9994 with a linear regression coefficient (zero intercept) of 3.7 x 10^{-7} cm^3_{STP} g^{-1} $‰^{-1}$) (Supplementary Figure S1). Thus, we hereafter interpret $\Delta^{40}Ar$ as equivalent to $^{40}Ar_{rad}$.

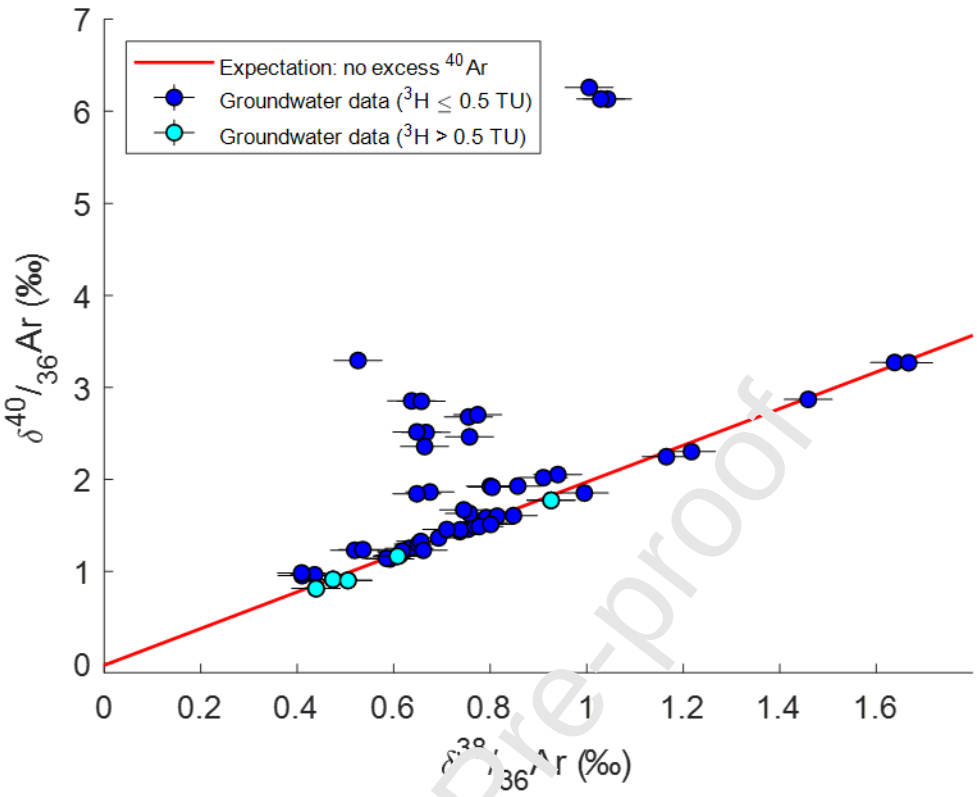

Figure 2: Measured $\delta^{40}/_{36}$Ar vs. $\delta^{38}/_{36}$Ar in California groundwater samples alongside the expected linear relationship for physical fractionation of atmosphere-derived argon (red line; same as in Figure 1). Samples with observed ^{3}H activities above 0.5 TU (i.e., dominated by post-1950s recharge) are represented as cyan circles, while all other samples are shown as dark blue circles. Error bars indicate measurement uncertainty (±2σ).

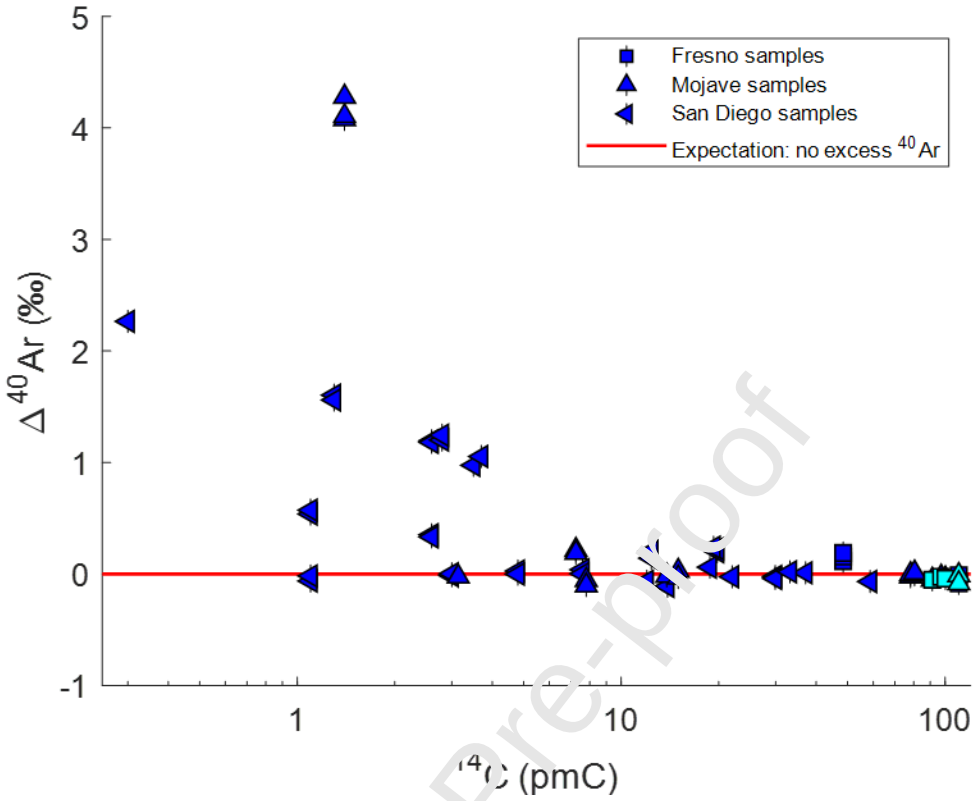

Figure 3: $\Delta^{40}Ar$ and ^{14}C activity of DIC across all samples analyzed in this study. Study areas are distinguished by marker type. Samples with observed ^{3}H activities above 0.5 TU are displayed in cyan, while all other samples are displayed in dark blue. Error bars indicate combined measurement and physical-model uncertainties for $\Delta^{40}Ar$ (±2σ). The red line indicates the expectation if all ^{40}Ar is atmosphere-derived (i.e., $\Delta^{40}Ar$=0), as shown in Figures 1 and 2.

In Figure 3, the highest observed $\Delta^{40}Ar$ value (> 4‰) is found in a Mojave Desert well and replicated in three separate samples. The highest observed $\Delta^{40}Ar$ among San Diego samples is +2.27‰, measured in a sample collected from a 607-m deep artesian monitoring well with negligible ^{14}C activity (<0.2 pmC). This well was previously found to have an ^{81}Kr activity of ~41% the modern atmospheric value, implying a mean age of ~300 ka (Seltzer et al., 2019b). In both San Diego and the Mojave Desert, some samples were found to contain no $^{40}Ar_{rad}$ ($\Delta^{40}Ar$=0), both in cases where ^{14}C activities were high (e.g., >50 pmC) and low (e.g., <10 pmC). In samples collected near Fresno, replicate samples from a shallow monitoring well (with

high ^{3}H and ^{14}C activities) were found to contain no excess radiogenic ^{40}Ar, while samples from a deeper supply well with a ^{14}C activity of ~50 pmC and negligible ^{3}H activity were observed to have small but significantly non-zero $\Delta^{40}Ar$ values (mean $\Delta^{40}Ar$ = +0.154‰, n=3). Given the small number of Fresno samples, we focus the remaining discussion on the San Diego and Mojave Desert systems.

4.2.1 Overview of $\Delta^{40}Ar$ and Hydrogeology in San Diego Groundwater System

In the San Diego groundwater system, we report $\Delta^{40}Ar$ measured in 35 samples collected from 23 scientific monitoring wells. As shown in Figure 4, these wells are distributed among six separate locations and each is screened at a distinct depth interval (screen opening ~6m), between ~50 and 600 meters below the land surface (mbls). The names of the six multiple-depth sites are shown alongside site-specific markers in Figure 4. The groundwater system consists of a shallow, unconfined aquifer and a deeper, regional confined aquifer (Anders et al., 2013). Both of these aquifers are composed of coastal sediments that progressively filled in the pull-apart basin formed by regional faulting (Keller and Ward, 2001) due to changes in sea-level and uplift over geological time (Hanson et al., 2009). Although the groundwater flow characteristics and pathways are under-constrained, the flow direction is generally westward, and recharge to the regional system is assumed to occur to the east of the wells sampled for this study near the transition from steep volcanic surficial geology to more permeable sediments (Flint et al., 2012; Seltzer et al., 2019b). While most old groundwater (^{14}C-derived mean ages > 10 ka) is found below 150 mbls, at the northernmost site (SDAQ), artesian wells containing old groundwater are found as shallow as 50 mbl (Supplementary Figure S3).

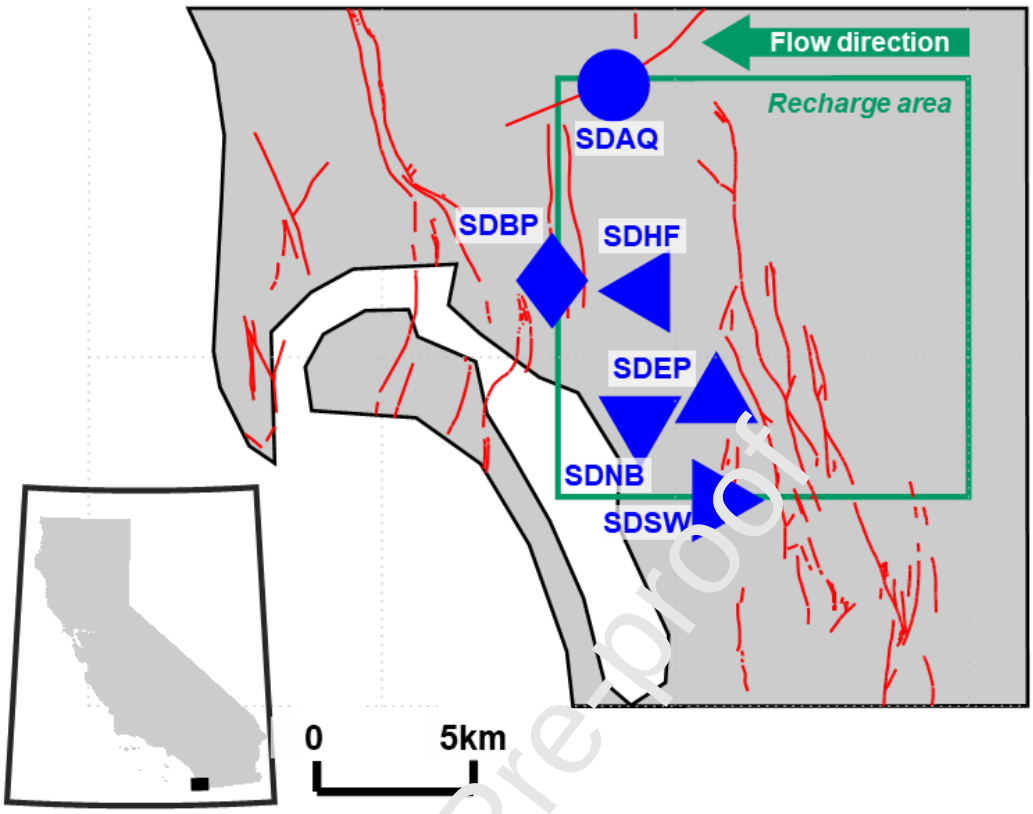

Figure 4: Map of San Diego groundwater system. Multiple-depth monitoring well site locations are indicated by blue markers, and the presumed recharge area boundary and predominant flow directions are indicated by the green box and arrow, respectively. Red lines indicate locations of quaternary faults (Haller et al., 2004). Inset: Location of study area within State of California.

In San Diego groundwater, replicate-mean $\Delta^{40}Ar$ ranges from -0.11 to +2.27‰. In general, we find that $\Delta^{40}Ar$ is positively correlated with well depth, groundwater age, and total dissolved solids (TDS). In Figure 5, replicate-mean $\Delta^{40}Ar$ is plotted against TDS, with marker shading corresponding to dissolved potassium concentrations. Several key patterns emerge from Figure 5 that are central to our interpretation of the predominant controls on $\Delta^{40}Ar$ in this system. First, we note that the seven wells with the lowest TDS, which are all below 950 mg L^{-1}, have zero $\Delta^{40}Ar$ within error. Similarly, the two highest $\Delta^{40}Ar$ values found in San Diego correspond to two of the three highest TDS values. Overall, the positive correlation between $\Delta^{40}Ar$ and TDS points towards weathering of aquifer minerals as a dominant mechanism by which $\Delta^{40}Ar$ is

released into groundwater. Notably, the dissolved potassium concentration appears largely unrelated to Δ^{40}Ar, as three of the highest observed K concentrations – corresponding to wells labeled a, b, and c in Figure 5 and subsequent figures – are associated with zero Δ^{40}Ar, within error. We emphasize that these three wells, which are from three distinct sites, also markedly deviate from the observed general trend between Δ^{40}Ar and TDS (Figure 5). These wells all have high TDS (between ~2000 and 2700 mg L^{-1}), but lack Δ^{40}Ar. Notably, these three wells also have apparent ^{14}C ages between ~10 and 20 ka and broadly plot along a linear depth-age trend (Supplementary Figure S3; R^2=0.80) that describes most wells (n=19), except the three shallowest artesian SDAQ wells and the >600-mbls deep, ~300 ka ^{81}Kr-dated well. Thus, we suggest that the anomalously low Δ^{40}Ar in wells a, b, and c is unrelated to groundwater age or flow, since the groundwater in these wells appears to have experienced similar water-rock interaction of comparable extent as other wells of similar depth and age.

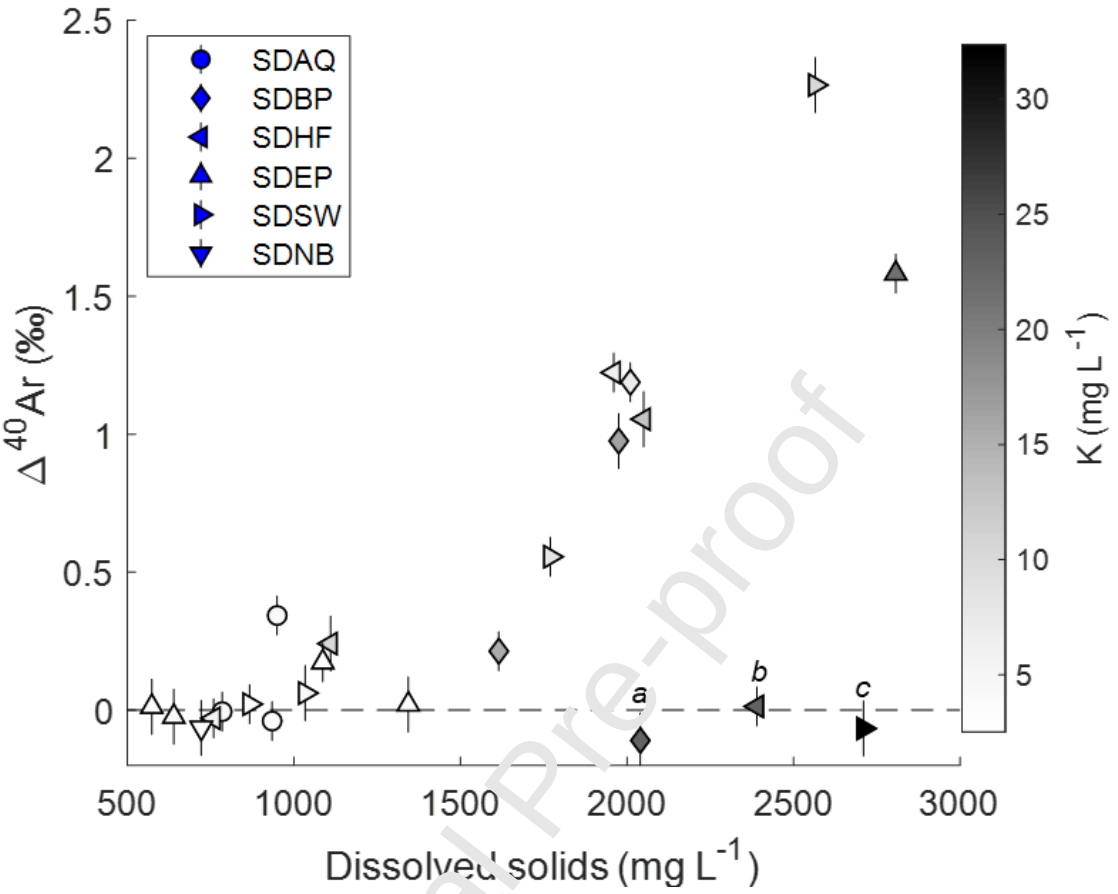

Figure 5: Replicate-mean $\Delta^{40}Ar$ versus total dissolved solids (TDS) in San Diego groundwater samples. Marker shapes correspond to multiple-depth sites and shading indicates dissolved potassium concentration. Wells a, b, and c, which are central to the interpretation of $\Delta^{40}Ar$ controls in this system, are specifically identified here and in later figures. Error bars indicate ±2 SE.

In Figure 6, replicate-mean $\Delta^{40}Ar$ is shown as a function of depth below the land surface, with marker shading proportional to ^{14}C-derived apparent groundwater ages (reported by Seltzer et al., 2019b). Note that the surface elevations of all the sites are similar (between 4 and 33 meters above sea level). In the four of the five wells shallower than 100 mbls, $\Delta^{40}Ar$ is zero (within error) and no well shallower than 300 mbls shows $\Delta^{40}Ar$ above +0.5‰. The three outlier wells identified in Figure 5 (a, b, c) are perforated at depth intervals within the ~150-300 mbls range, in which several other samples with apparent ^{14}C ages >10 ka have small but statistically

non-zero Δ^{40}Ar values. Notably, Δ^{40}Ar is ≥ +1‰ in 7 of 23 total wells, all of which have perforated depth intervals below 300 mbls.

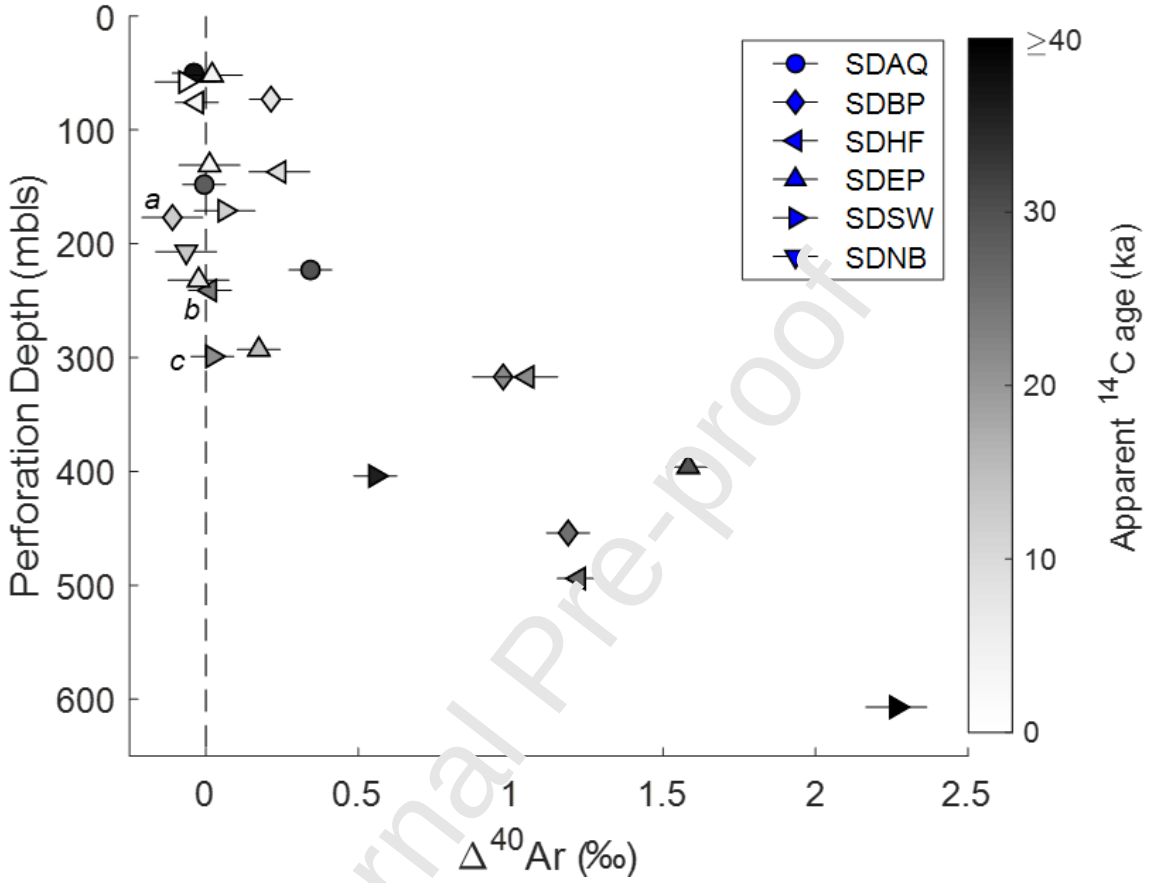

Figure 6: Depth trends in replicate-mean Δ^{40}Ar from San Diego groundwater samples. Marker shapes correspond to multiple-depth sites and shading indicates apparent ^{14}C age (Seltzer et al., 2019b). Error bars indicate ±2 SE.

4.2.2. Discussion of mechanistic controls on Δ^{40}Ar in San Diego

In light of the observed relationships between Δ^{40}Ar, apparent ^{14}C age of groundwater, and TDS, we suggest that the accumulation of ^{40}Ar in San Diego groundwater depends upon three key factors: (i) a long (order 10 ka) groundwater residence time and both (ii) high weatherability and (iii) old age of aquifer minerals along the integrated flow path of groundwater in the system. When any of these conditions is not met, Δ^{40}Ar appears to be negligible. Below,

we briefly outline three examples within the San Diego groundwater data set in which $\Delta^{40}Ar$ is low and evidence suggests that one of these conditions is not satisfied.

First, based on Figures 5 and 6, we point out that all shallow (<100 m), young (<10 ka ^{14}C age), low TDS (<1000 mg L^{-1}) samples have negligible $\Delta^{40}Ar$. Put simply, we suggest that young groundwaters have experienced limited opportunity to dissolve aquifer minerals and thereby liberate radiogenic ^{40}Ar from K-bearing minerals. Second, we focus on the three SDAQ wells, which range in apparent ^{14}C age from ~28 to 37 ka (Supplementary Figure S3) but all have low $\Delta^{40}Ar$ values and TDS < 1000 mg L^{-1} (Figures 5 and 6). The SDAQ wells are anomalous, in that they are shallower than other wells containing similarly old groundwater (Supplementary Figure S3) and they are located further north than the other multiple-depth well sites (Figure 4). The flow path of SDAQ wells is distinct from other wells, in that the relatively shallow, slow flow of these order ten-thousand year old waters likely passed through primarily metavolcanic rocks before flowing to the Eocene sedimentary formation that begins only several kilometers to the east of the SDAQ site. Because metavolcanic rocks are considerably less weatherable than sedimentary formations, we suggest that the unique flow path of these groundwaters explains both their anomalously low TDS and low $\Delta^{40}Ar$ for their high apparent ^{14}C ages. Third, we call attention to the outlier wells in Figure 5 (a, b, and c), which contain old (>10 ka) groundwater with high TDS but zero $\Delta^{40}Ar$.

The co-occurrence of high TDS and zero $\Delta^{40}Ar$ in these old groundwater samples implies that these groundwaters have exclusively interacted with either young or K-poor aquifer minerals. Either condition would lead to ^{40}Ar-poor aquifer minerals that are inherently unable to release substantial ^{40}Ar to groundwater upon weathering. To the extent that the dissolved major element composition of high-TDS groundwater reflects the source composition of aquifer

minerals that were dissolved over the lifetime of groundwater in the aquifer, we can rule out the latter hypothesis (K-poor minerals) based on comparison of $\Delta^{40}Ar$ to dissolved K concentrations (Figure 5). While no clear overall trend is apparent, several important features are notable. First, $\Delta^{40}Ar$ is zero for nearly all cases in which K concentrations are low (<6 mg L^{-1}). Second, the highest observed $\Delta^{40}Ar$ value is associated with an intermediate K concentration. Third, and most notably, the three highest observed K concentrations correspond to the low $\Delta^{40}Ar$, high-TDS samples of interest (a, b, and c). Taken together, these observations strongly suggest that the closure age of K-bearing minerals (i.e., the time at which K-bearing minerals originally reached their closure temperature and began to accumulate radiogenic ^{40}Ar), rather than the overall K content of dissolved aquifer minerals, controls the $\Delta^{40}Ar$ of groundwater in this system.

In the broader context of the geological differences among the six multiple-depth well sites, these considerations further support the conclusion that ^{40}Ar in groundwater is predominantly derived from weathering of old aquifer minerals. For instance, among wells of comparable ^{14}C age, no apparent relationship exists between $\Delta^{40}Ar$ and the proximity of well locations (or their associated east-west flowlines) to known Quaternary faults (e.g., Figures 4 and 6) or ^{14}C age (Supplementary Figure S3). Whereas faults might provide efficient conduits for a flux of crustal radiogenic gases like ^{4}He, which readily diffuses from minerals into groundwater (Solomon, 2000), the diffusive loss of ^{40}Ar (which is heavier and larger than ^{4}He) at cold temperatures (<200°C) is known to be minimal (Andrews et al., 1989). Conversely, faults can act as effective seals, thereby isolating groundwater from a hypothetical crustal ^{40}Ar flux. If either scenario were to have been the case in the San Diego groundwater system, we might have expected to see a coherent relationship between $\Delta^{40}Ar$ and proximity to faults.

4.2.3. Potential Source of ^{40}Ar in Deep San Diego Groundwater

We observe a compelling relationship between $\Delta^{40}Ar$ and the stratigraphy of sedimentary formations at each site, as reported by the U.S. Geological Survey based on core logs (Figure 7). Briefly, five main sedimentary units of spatially varying extents and thicknesses exist across the 0-600 mbls depth range within the study area: Quaternary sediments, the upper and lower San Diego formation, the Otay formation, and various Eocene formations. Below the Quaternary sediments, which are present at each site but highly variable in thickness, the San Diego Formation is found at all sites except for SDAQ. The San Diego formation consists of two units formed in the Pliocene: 1) an upper unit that is both marine and non-marine, consisting of fine- and coarse-grained sandstones as well as thick conglomerates, and 2) a lower unit consisting of marine sediments including fine-grained sandstones and thin conglomerates (Demere, 1983). Below the San Diego formation is the Otay formation, which was formed in the Oligocene and consists of a bottom conglomerate layer, middle gritstone layer, and upper sandstone/mudstone layer (Walsh and Demere, 1991). Waxy bentonites are abundant in the upper-layer and have been dated to the Oligocene (Berry, 1999). Finally, sandstone units formed during the Eocene (Kennedy et al., 2008) are found below the Otay formation at SDSW, SDBP, and SDHF, and directly below the Quaternary sediments at SDAQ.

As shown in Figure 7, we find that six of the seven wells for which $\Delta^{40}Ar$ is ≥ 1‰ have perforated depth intervals within Eocene sedimentary formations. Perhaps, the most striking example of the relationship between stratigraphy and $\Delta^{40}Ar$ is seen in wells at ~300 mbls (±17 m) at the SDBP, SDHF, SDEP and SDSW sites (purple box in Figure 7). Whereas the groundwater samples from these four wells are similar in age (~20 ka; Supplementary Figure S3), samples from wells perforated within the Eocene formations (SDBP, SDHF) have $\Delta^{40}Ar$

~1.0‰ (Figure 6), while both samples from wells perforated above the Eocene formations (SDEP, SDSW) have virtually no radiogenic ^{40}Ar ($\Delta^{40}Ar < 0.18$‰; Figure 7).

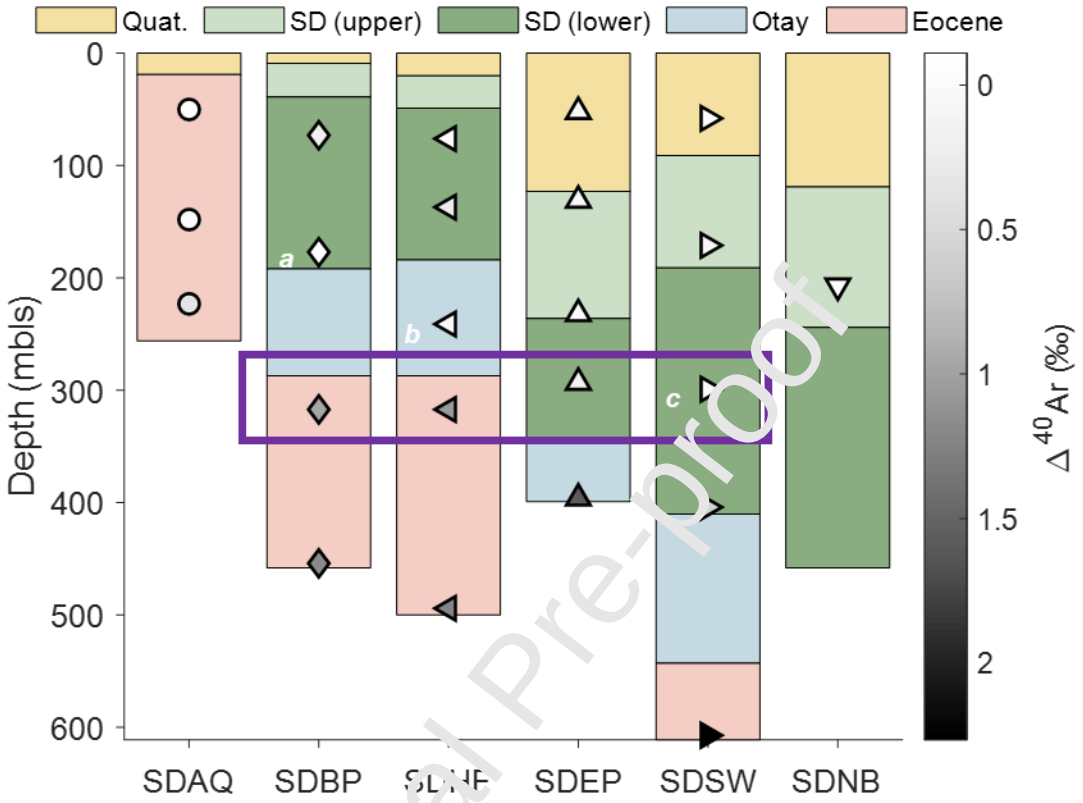

Figure 7: Stratigraphy at each multiple-depth well site (map provided in Figure 4). The lowest reported depth at each site indicates the maximum drilling depth. Markers indicate perforated depth intervals of wells sampled in this study, and marker shading corresponds to $\Delta^{40}Ar$. Notably, all wells with $\Delta^{40}Ar \geq 1$‰ are perforated within the Eocene formations or deep Otay formation (in the single case of the deepest SDEP well). The purple box indicates samples at comparable depths (~200 mbls) with markedly different $\Delta^{40}Ar$ values. Note that the depth interval associated with Eocene sediments is unknown at the SDEP site because the bottom of the drilling core was within the Otay formation.

Why is $\Delta^{40}Ar$ so strongly associated with Eocene sandstone units? To explore the link between these geological formations and $\Delta^{40}Ar$, we consider the broader regional geological background and suggest that the presence of >1 Ga-old K-feldspar within the Eocene sandstone units is likely source of ^{40}Ar. Late Cretaceous-Tertiary forearc stratigraphic sequences in coastal southern California and northern Baja California are characterized by a distinct late-Paleocene/late-Eocene provenance shift from local to extra-regional sediment input sources

(Ingersoll et al., 2013). Turonian-Maastrichtian forearc strata were derived from local Cretaceous Peninsular Ranges magmatic arc sources in association with progressive ~5-15 km of erosional unroofing of the batholith (Grove et al., 2003). The subsequent transition to Laramide flat-slab subduction (~75-55 Ma) allowed for eastward expansion of drainages into the Jurassic arc/Proterozoic crystalline basement of southwest Laurentia, and transport of this extra-regional sediment westwards to the coast across low relief erosional surfaces of the Peninsular Ranges. Late-Eocene/earliest-Oligocene surface uplift in the northern Peninsular Ranges associated with east-side-up reactivation of late Cretaceous structures disrupted and rerouted these extra-regional rivers (Axen et al., 2000), so that from the Oligocene through the Pliocene, local sources of sand again dominated in southern California (Ingersoll et al., 2013).

The extra-regional nature of late-Paleocene/late-Eocene sediment was first documented by the presence of mid-Jurassic age rhyolite clasts in fluvial-alluvial sequences; these include the conspicuous Eocene Poway-type red rhyolite clasts in San Diego (Abbott and Smith, 1989). Subsequently, detrital zircon U-Pb provenance analysis has been widely applied through the southern California Late Cretaceous-Tertiary sequences (Ingersoll et al., 2013, 2018; Sharman et al., 2014). The application of detrital zircon geochronology allows for expansion of provenance analysis to include sandstone, and particularly marine sandstone sequences that are the dominant lithological component of the Paleocene-Eocene sequences. A recent study applied U/Pb dating to extra-regional detrital zircon in Eocene sandstone strata in San Diego from five separate samples: two from fluvial-alluvial sandstone interbedded from Poway Group conglomerates, and three from shallow marine sandstone of the La Jolla Group (Sharman et al., 2014). A histogram of extra-regional zircon U/Pb ages shows a major peak at ~1700 Ma and a secondary peak at ~1400 Ma (Supplementary Figure S4). Cratonal basement sources for these zircon include

voluminous granite and granodiorite that would have supplied biotite and K-feldspar to the southern California extra-regional rivers. K-feldspar is relatively resistant to both weathering and in situ diagenetic alteration compared to plagioclase, or biotite which readily undergoes weathering to chlorite. Overall, the five samples analyzed by Shaman et al. (2014) contain 30-50% Proterozoic zircon, implying that substantial percentages of Proterozoic detrital K-feldspar should also be present in these Eocene strata.

While the ratio of extra-regional Proterozoic detrital zircon to K-feldspar in San Diego Eocene sandstones is unknown, we can draw inferences from an analogous geologic setting. Late Cretaceous forearc strata of the Nainamo basin in southern British Columbia experienced a closely comparable local to extra-regional provenance shift to the Southern California forearc sequences. There, 54% of the extra-regional detrital zircon is Proterozoic age, and 47% of the detrital K-feldspar yield $^{40}Ar/^{39}Ar$ ages defining a continuous distribution up to 1.03 Ga that are interpreted as partially degassed Proterozoic K-feldspar (Isava et al., 2021). The implication is that detrital K-feldspar is present is approximately equivalent abundance to Proterozoic zircon. An ongoing study in the northern Santa Ana Mountains also demonstrates the presence of partially outgassed Proterozoic K-feldspar in Eocene sandstone units that is absent from underlying and overlying locally sourced facies (Grove, person. com., 2021).

How much dissolution of Proterozoic K-feldspar in Eocene sandstone would be required to produce the observed groundwater $\Delta^{40}Ar$ signals? As an illustrative (non-unique) example, we calculate an expected $\Delta^{40}Ar$ value of +0.96‰ if a parcel of groundwater dissolves 0.01% of aquifer rock within the Eocene strata. In our idealized calculation, we assume that one third of the K within the Eocene strata has an age consistent with the peak in the zircon U/Pb age distribution (1.7 Ga). We also assume 20% aquifer porosity, 5% K content, a ^{40}K decay

branching ratio (to ^{40}Ar versus ^{40}Ca) of 0.1048 (Marshall, 2006), a uniform aquifer rock bulk density of 2.5 g cm^{-3}, and an initial (atmosphere-derived) ^{40}Ar content of groundwater equal to air-saturated freshwater at 1 atm and 20°C (Jenkins et al., 2019). The details of the calculation are provided in Appendix A. While these input parameters are underconstrained, our calculation in principle supports the notion that weathering of Proterozoic K-feldspar in Eocene strata is a plausible source of the $\Delta^{40}Ar$ we observe in San Diego groundwater. Importantly, this calculation satisfies mass balance considerations. For example, extrapolating the weathering rate by assuming a mean groundwater residence time of 30 ka and lithification age of Eocene strata of 30 Ma implies that ~10% of Eocene deposited units may have dissolved over time. A corollary to this result from San Diego is that similar or greater groundwater ^{40}Ar anomalies might be expected from the Los Angeles basin and surrounding areas (McCulloch et al., 2000) where Eocene extra-regional strata in general has greater proportions of Proterozoic zircon compared to San Diego, with individual samples containing >70% Proterozoic zircon in the Los Angeles basin.

4.3. Insights from Paired ^{40}Ar and He measurements in the Mojave Desert

In the western Mojave Desert, 18 groundwater samples were collected from 11 supply wells across a wide spatial extent (from 34.4 to 35.0 °N and from 117.4 to 118.1 °W). We find that replicate-mean $\Delta^{40}Ar$ ranges from virtually zero to +4.2‰, with the latter value replicated in three samples from the same well (Figure 8). Notably, $\Delta^{40}Ar$ is significantly non-zero in samples from only two of 11 Mojave Desert wells. Given the limited number of samples, the potential for mixing due to the long perforated depth intervals of some wells, and the spatially wide study area that encompasses multiple shallow local and deep regional flow systems from the Mojave River

Basin (Kulongoski et al., 2009, 2003) and Antelope Valley groundwater system (Siade et al., 2014), we are unable to provide a comprehensive analysis of the Mojave Desert samples. Nonetheless, because ^{4}He and ^{14}C data exist from past U.S. Geological Survey measurements (Arnold et al., 2018, 2016), we briefly discuss the correspondence between $\Delta^{40}Ar$ and these two groundwater age tracers.

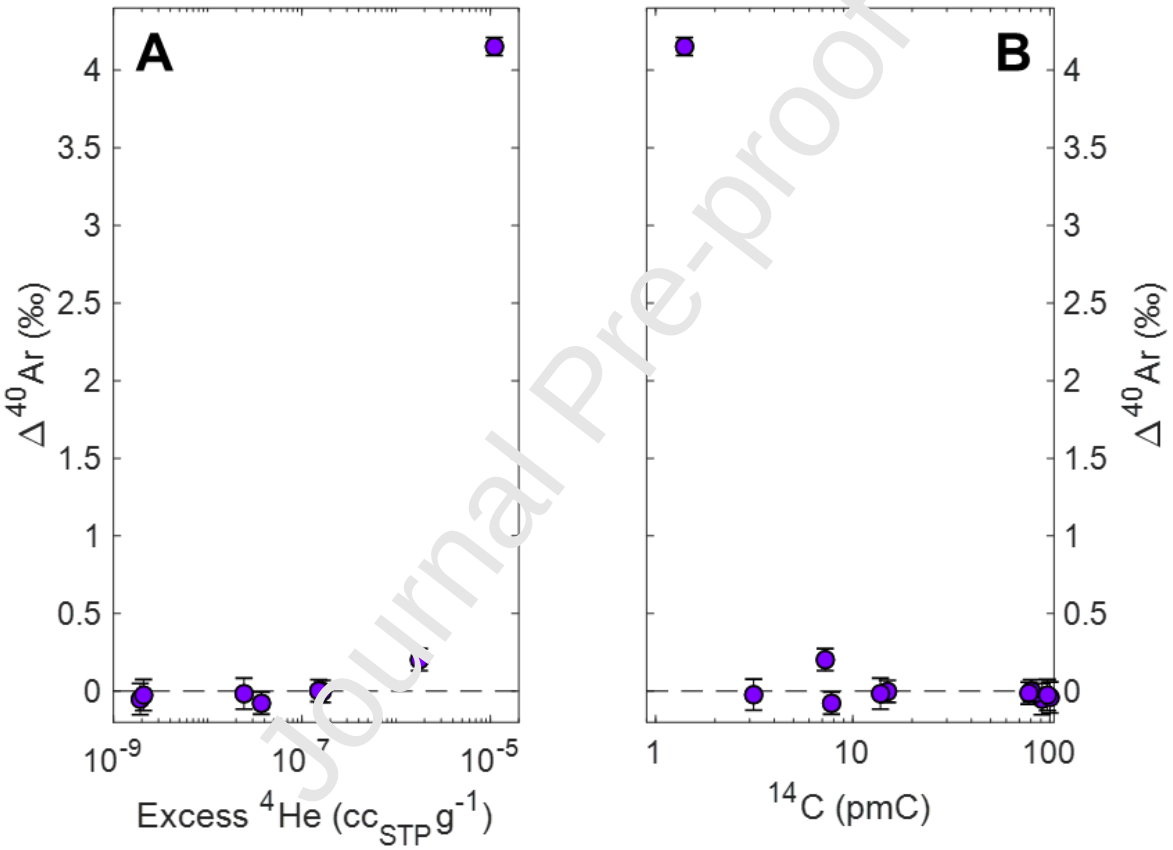

Figure 8: Mojave Desert replicate-mean $\Delta^{40}Ar$ versus excess ^{4}He (panel A) and ^{14}C activity (panel B). Note that excess ^{4}He data are available for only 8 of 11 total Mojave Desert wells sampled for Ar isotope analysis, while ^{14}C data are available for all 11 wells. Error bars indicate ±2 SE.

Using measured Ne, Ar, Kr, and Xe data and the PANGA software (Jung and Aeschbach, 2018), we determine the expected non-radiogenic ^{4}He concentrations (i.e., from air-saturated water and excess air) by assuming a recharge elevation of 1100 m (Kulongoski et al., 2009) and

by employing the Closed-system Equilibration (CE) model (Aeschbach-Hertig et al., 2000). We then determined excess ^{4}He by subtracting non-radiogenic ^{4}He from measured ^{4}He. As shown in Figure 8, we observe a four order-of-magnitude range of variability in excess ^{4}He, and find that the two highest excess ^{4}He values (1.1 x 10^{-5} cm^{3}_{STP} g^{-1}, 1.8 x 10^{-6} cm^{3}_{STP} g^{-1}) correspond to the two highest Δ^{40}Ar values (4.2‰, 0.2‰). Similarly, the well with the highest excess ^{4}He and Δ^{40}Ar also shows the lowest ^{14}C activity of DIC (1.4 pmC). However, the relationship between Δ^{40}Ar and groundwater age is clearly complex across this large region with variable groundwater flow and lithology, as four of the six wells containing groundwater with ^{14}C activities below 11 pmC have Δ^{40}Ar values of zero (Figure 8). In light of this complexity, we suggest that groundwater age is clearly a first-order control on Δ^{40}Ar in the western Mojave Desert, as is the case in San Diego. The weatherability and age of aquifer minerals are also likely to play key roles in setting Δ^{40}Ar in the Mojave.

5. Conclusions

In this study, we have detected robust, non-zero signals of radiogenic ^{40}Ar in order ten-thousand-year-old groundwater for the first time from multiple study areas in California. By using the non-radiogenic Ar isotopes to correct for physical fractionation processes that impact ^{40}Ar, we have successfully isolated radiogenic signals and demonstrated that our model is physically valid, finding only positive values of Δ^{40}Ar (within uncertainty) that occur exclusively in ^{3}H-free, low ^{14}C groundwater. In a network of 23 scientific monitoring wells in San Diego – the most extensive portion of this study – we have found compelling evidence linking ^{40}Ar accumulation in groundwater to weathering of old, K-bearing minerals. Based on the San Diego data, we suggest that the presence of ^{40}Ar requires three factors: (i) aquifer minerals high in K,

which have been (ii) sufficiently aged and weathered, and (iii) groundwater residence times long enough for water-rock interactions to dissolve the K-rich aquifer minerals. Our observations in the western Mojave Desert, though limited in number, are compatible with these observations. We note that our argument in favor of an exclusive weathering control on ^{40}Ar accumulation in groundwater, rather than a diffusive flux from aquifer minerals, is also consistent with prior work (Andrews et al., 1989).

We suggest that $\Delta^{40}Ar$ may represent a useful complementary tracer to ^{4}He and ^{14}C in future studies of Late Pleistocene groundwater. For example, because excess ^{4}He is thought to be predominantly controlled by diffusion from aquifer minerals (Solomon, 2000), groundwater that has interacted only with poorly weatherable U- and Th-bearing minerals might contain excess ^{4}He but lack excess ^{40}Ar, if ^{40}Ar accumulation is primarily controlled by weathering. In this sense, coupled with a general understanding of the stratigraphy and geochemical composition of aquifer minerals, the combined application of ^{4}He and triple Ar isotopes may provide insight into the integrated lithology along a given groundwater flow path. Similarly, whereas ^{14}C of DIC is arguably the most widely used dating tool for Late Pleistocene groundwater, it suffers from dilution of the DIC ^{14}C pool by introduction of ^{14}C-free DIC from water-rock interaction (Cartwright et al., 2020). To the extent that $\Delta^{40}Ar$ reflects integrated weathering of aquifer minerals, it may provide additional insight (along with $\delta^{13}C$) into the deconvolution of ^{14}C signals in groundwater and thereby improve the accuracy of groundwater dating with ^{14}C. Finally, we note that high-precision measurements of $\Delta^{40}Ar$ may also aid in constraining nucleogenic ^{39}Ar input to groundwater. For young groundwater (<1500 years), $\Delta^{40}Ar$ may serve as a proxy for nucleogenic ^{39}Ar and thereby provide additional confidence in the use of atmosphere-derived ^{39}Ar to date groundwater (e.g., Loosli, 1983). For example, where $\Delta^{40}Ar > 0$,

^{39}Ar ages that assume only an atmospheric source of ^{39}Ar should be treated with caution. On longer timescales, the ratio of nucleogenic ^{39}Ar to radiogenic ^{40}Ar is a promising, yet underutilized, tracer of fluid-rock interaction and groundwater residence time that may benefit from high-precision measurements of Δ^{40}Ar (Yokochi et al., 2012). We therefore recommend the inclusion of triple argon isotope measurements in future studies as a valuable complement to (a) ^{14}C and ^{4}He in Late Pleistocene-aged groundwater, and (b) ^{39}Ar on both short (centennial) and long (>10 ka) timescales.

Acknowledgements: We dedicate this manuscript to the late Dave Hilton, who was an early proponent of the technique for high-precision noble gas isotope measurements in groundwater and served on the thesis committee of AS, who developed the analytical method during his PhD at Scripps Institution of Oceanography. Dave was also a great mentor, colleague, and friend to many of the authors, and we are grateful for his many contributions to the field of groundwater noble gas geochemistry. We also thank Martin Stute and Marty Grove for helpful discussions. This work was supported in part by NSF-EAR-1702704 (to JS), NSF-EAR-1702571 (to MS), and NSF-OCE-1923915 (to AS and PB), and the U.S. Geological Survey Cooperative Water Program.

6. References

Abbott, P.L. and Smith, T.E., 1989, Sonora, Mexico, source for the Eocene Poway Conglomerate of southern California, Geology v. 17, p. 329-332.Aeschbach-Hertig, W., Peeters, F., Beyerle, U., Kipfer, R., 2000. Palaeotemperature reconstruction from noble gases in ground water taking into account equilibration with entrapped air. Nature 405, 1040–4.

doi:10.1038/35016542

Aeschbach-Hertig, W., Solomon, D.K., 2013. Noble Gas Thermometry in Groundwater Hydrology, in: The Noble Gases as Geochemical Tracers. Springer Berlin Heidelberg, Berlin, Heidelberg, pp. 81–122. doi:10.1007/978-3-642-28836-4_5

Aeschbach-Hertig, W., Stute, M., Clark, J.F., Reuter, R.F., Schlosser, P., 2002. A paleotemperature record derived from dissolved noble gases in groundwater of the Aquia Aquifer (Maryland, USA). Geochim. Cosmochim. Acta 66, 797–817. doi:10.1016/S0016-7037(01)00804-3

Aggarwal, P.K., Matsumoto, T., Sturchio, N.C., Chang, H.K., Gastmans, D., Araguas-Araguas, L.J., Jiang, W., Lu, Z.-T., Mueller, P., Yokochi, R., Purtschert, R., Torgersen, T., 2015. Continental degassing of 4 He by surficial discharge of deep groundwater. doi:10.1038/NGEO2302

Anders, R., Mendez, G.O., Futa, K., Danskin, W.R., 2014. A Geochemical Approach to Determine Sources and Movement of Saline Groundwater in a Coastal Aquifer. Groundwater 52, 756–768. doi:10.1111/gwat.12108

Andrews, J.N., Hussain, N., Youngman, M.J., 1989. Atmospheric and radiogenic gases in groundwaters from the Stripa granite. Geochim. Cosmochim. Acta 53, 1831–1841. doi:10.1016/0016-7037(89)90304-9

Andrews, J.N., Lee, D.J., 1979. Inert gases in groundwater from the Bunter Sandstone of England as indicators of age and palaeoclimatic trends. J. Hydrol. 41, 233–252. doi:10.1016/0022-1694(79)90064-7

Arnold, T.L., Bexfield, L.M., Musgrove, M., Stackelberg, P.E., Lindsey, B.D., Kingsbury, J.A., Kulongoski, J.T., Belitz, K., 2018. Groundwater-quality and select quality-control data from

the National Water-Quality Assessment Project, January through December 2015, and previously unpublished data from 2013 to 2014, Data Series. doi:10.3133/ds1087

Arnold, T.L., Desimone, L.A., Bexfield, L.M., Lindsey, B.D., Barlow, J.R.B., Kulongoski, J.T., Musgrove, M., Kingsbury, J.A., Belitz, K., 2016. Groundwater quality data from the National Water-Quality Assessment Project, May 2012 through December 2013, Data Series. doi:10.3133/ds997

Ballentine, C.J., Burnard, P.G., 2002. Production, release and transport of noble gases in the continental crust. Rev. Mineral. Geochemistry 47. doi:10.2138/rmg.2002.47.12

Befus, K.M., Jasechko, S., Luijendijk, E., Gleeson, T., Bayani Cardenas, M., 2017. The rapid yet uneven turnover of Earth's groundwater. Geophys. Res. Lett. 44, 5511–5520. doi:10.1002/2017GL073322

Bender, M.L., Barnett, B., Dreyfus, G., Jouzel, J., Porcelli, D., 2008. The contemporary degassing rate of 40Ar from the solid Earth. Proc. Natl. Acad. Sci. U. S. A. 105, 8232–7. doi:10.1073/pnas.0711679105

Berry, R.W., 1999. Eocene and Oligocene otay-type waxy bentonites of San Diego County and Baja California: Chemistry, mineralogy, petrology and plate tectonic implications. Clays Clay Miner. 47, 70–83. doi:10.1346/CCMN.1999.0470108

Bethke, C.M., Johnson, T.M., 2008. Groundwater Age and Groundwater Age Dating. doi:10.1146/annurev.earth.36.031207.124210

Beyerle, U., Aeschbach-Hertig, W., Imboden, D.M., Baur, H., Graf, T., Kipfer, R., 2000. A mass, spectrometric system for the analysis of noble gases and tritium from water samples. Environ. Sci. Technol. 34, 2042–2050. doi:10.1021/es990840h

Bourg, I.C., Sposito, G., 2008. Isotopic fractionation of noble gases by diffusion in liquid water:

Molecular dynamics simulations and hydrologic applications. Geochim. Cosmochim. Acta 72, 2237–2247. doi:10.1016/j.gca.2008.02.012

Cartwright, I., Currell, M.J., Cendón, D.I., Meredith, K.T., 2020. A review of the use of radiocarbon to estimate groundwater residence times in semi-arid and arid areas. J. Hydrol. doi:10.1016/j.jhydrol.2019.124247

Clark, J.F., Stute, M., Schlosser, P., Drenkard, S., Bonani, G., 1997. A tracer study of the Floridan Aquifer in southeastern Georgia: Implications for groundwater flow and paleoclimate. Water Resour. Res. 33, 281–289. doi:10.1029/96WR03017

COESA, 1976. U.S. Standard Atmosphere. Washington, D.C.

Deeds, D.A., Vollmer, M.K., Kulongoski, J.T., Miller, B.R., Mühle, J., Harth, C.M., Izbicki, J.A., Hilton, D.R., Weiss, R.F., 2008. Evidence for crustal degassing of CF4 and SF6 in Mojave Desert groundwaters. Geochim. Cosmochim. Acta 72, 999–1013. doi:10.1016/j.gca.2007.11.027

Demere, T.A., 1983. The Neogene San Diego Basin: A Review of the Marine Pliocene San Diego Formation, in: Cenozoic Marine Sedimentation Pacific Margin, U.S.A. Pacific Section SEPM, pp. 187–195.

Fishman, M.J., 1993. Methods of analysis by the U.S. Geological Survey National Water Quality Laboratory; determination of inorganic and organic constituents in water and fluvial sediments. U.S. Geol. Surv. Open File Rep. 93-125 217.

Flint, L.E., Flint, A.L., Stolp, B.J., Danskin, W.R., 2012. A basin-scale approach for assessing water resources in a semiarid environment: San Diego region, California and Mexico. Hydrol. Earth Syst. Sci. 16, 3817–3833. doi:10.5194/hess-16-3817-2012

Garbarino, J.R., Kanagy, L.K., Cree, M.E., 2006. Determination of elements in natural-water,

biota, sediment, and soil samples using collision/reaction cell inductively coupled plasma-mass spectrometry. U.S. Geological Survey, Reston, VA.

Gleeson, T., Befus, K.M., Jasechko, S., Luijendijk, E., Cardenas, M.B., 2016. The global volume and distribution of modern groundwater. Nat. Geosci. doi:10.1038/ngeo2590

Grachev, A.M., Severinghaus, J.P., 2003. Determining the thermal diffusion factor for 40Ar/36Ar in air to aid paleoreconstruction of abrupt climate change. J. Phys. Chem. A 107, 4636–4642. doi:10.1021/jp027817u

Haller, K.M., Machette, M.N., Dart, R.L., Rhea, B.S., 2004. U.S. Quaternary fault and fold database released. Eos, Trans. Am. Geophys. Union. doi:10.1029/2004eo220004

Hanson, R.T., Izbicki, J.A., Reichard, E.G., Edwards, B.D., Land, M., Martin, P., 2009. Comparison of groundwater flow in Southern California coastal aquifers, in: Earth Science in the Urban Ocean: The Southern California Continental Borderland. Geological Society of America, pp. 345–373. doi:10.1130/2009.2454(5.3)

Heaton, T.H.E., Vogel, J.C., 1981. "Excess air" in groundwater. J. Hydrol. doi:10.1016/0022-1694(81)90070-6

Higgins, J.A., Kurbatov, A.V., Spaulding, N.E., Brook, E., Introne, D.S., Chimiak, L.M., Yan, Y., Mayewski, P.A., Bender, M.L., 2015. Atmospheric composition 1 million years ago from blue ice in the Allan Hills, Antarctica. Proc. Natl. Acad. Sci. U. S. A. 112, 6887–6891. doi:10.1073/pnas.1420232112

Holland, G., Lollar, B.S., Li, L., Lacrampe-Couloume, G., Slater, G.F., Ballentine, C.J., 2013. Deep fracture fluids isolated in the crust since the Precambrian era. Nature 497, 357–360. doi:10.1038/nature12127

Hunt, A.G., 2015. U.S. Geological Survey Noble Gas Laboratory's standard operating

procedures for the measurement of dissolved gas in water samples, Techniques and Methods. doi:10.3133/tm5a11

Jasechko, S., Perrone, D., Befus, K.M., Bayani Cardenas, M., Ferguson, G., Gleeson, T., Luijendijk, E., McDonnell, J.J., Taylor, R.G., Wada, Y., Kirchner, J.W., 2017. Global aquifers dominated by fossil groundwaters but wells vulnerable to modern contamination. Nat. Geosci. 10, 425–429. doi:10.1038/ngeo2943

Jenkins, W.J., Lott, D.E., Cahill, K.L., 2019. A determination of atmospheric helium, neon, argon, krypton, and xenon solubility concentrations in water and seawater. Mar. Chem. 211, 94–107. doi:10.1016/j.marchem.2019.03.007

Jung, M., Aeschbach, W., 2018. A new software tool for the analysis of noble gas data sets from (ground)water. Environ. Model. Softw. 103, 120–130. doi:10.1016/j.envsoft.2018.02.004

Keller, B., Ward, A., 2001. Tectonic setting of the San Diego formation aquifer, considered for conjunctive use storage. J. South Am. Earth Sci. 14, 533–540. doi:10.1016/S0895-9811(01)00052-9

Kennedy, M.P., Tan, S.S., Bovard, K.R., Garcia, A.G., Burns, D., Gutierrez, C.I., Schwarzenegger, A., Luther, B., Parrish, J.G., 2008. Geologic Map of the San Diego 30’ x 60’ Quadrangle, California Digital Preparation by 2008 Prepared in cooperation with.

Kulongoski, J.T., Hilton, D.R., 2012. Applications of Groundwater Helium, in: Advances in Isotope Geochemistry. pp. 285–304. doi:10.1007/978-3-642-10637-8_15

Kulongoski, J.T., Hilton, D.R., Izbicki, J.A., 2005. Source and movement of helium in the eastern Morongo groundwater Basin: The influence of regional tectonics on crustal and mantle helium fluxes. Geochim. Cosmochim. Acta 69, 3857–3872. doi:10.1016/j.gca.2005.03.001

Kulongoski, J.T., Hilton, D.R., Izbicki, J.A., 2003. Helium isotope studies in the Mojave Desert, California: implications for groundwater chronology and regional seismicity. Chem. Geol. 202, 95–113. doi:10.1016/j.chemgeo.2003.07.002

Kulongoski, J.T., Hilton, D.R., Izbicki, J.A., Belitz, K., 2009. Evidence for prolonged El Nino-like conditions in the Pacific during the Late Pleistocene: a 43ka noble gas record from California groundwaters. Quat. Sci. Rev. 28, 2465–2473. doi:10.1016/j.quascirev.2009.05.008

Lippmann, J., Stute, M., Torgersen, T., Moser, D.P., Hall, J.A., Lin, L., Borcsik, M., Bellamy, R.E.S., Onstott, T.C., 2003. Dating ultra-deep mine waters with noble gases and 36Cl, Witwatersrand Basin, South Africa. Geochim. Cosmochim. Acta 67, 4597–4619. doi:10.1016/S0016-7037(03)00414-9

Loosli, H.H., 1983. A dating method with 39Ar. Earth Planet. Sci. Lett. 63, 51–62. doi:10.1016/0012-821X(83)90021-3

Marshall, B.D., 2006. Potassium-calcium decay system, in: Geochemistry. Kluwer Academic Publishers, pp. 525–526. doi:10.1007/1-4020-4496-8_260

Marty, B., Zimmermann, J., 1999. Volatiles (He, C, N, Ar) in mid-ocean ridge basalts: assesment of shallow-level fractionation and characterization of source composition. Geochim. Cosmochim. Acta 63, 3619–3633. doi:10.1016/S0016-7037(99)00169-6

Mazor, E., 1972. Paleotemperatures and other hydrological parameters deduced from noble gases dissolved in groundwaters; Jordan Rift Valley, Israel. Geochim. Cosmochim. Acta 36, 1321–1336. doi:10.1016/0016-7037(72)90065-8

McDougall, I., Harrison, T.M., 1999. Geochronology and thermochronology by the 40Ar/39Ar method, 2nd edition, Oxford University Press. Oxford.

N Andrews, C.J., Drimmie, R.J., Loosli, H.H., Hendry, M.J., 1991. Dissolved gases in the Milk River aquifer, Applied Geochemistry.

Oestlund, H.G., Dorsey, H.G., 1977. Rapid electrolytic enrichment and hydrogen gas proportional counting of tritium.

Revesz, K., Buck, B., Coplen, T.B., 2009. Determination of the δ(2H/1H) and δ(18O/16O)of Soil Water and Plant Matter: RSIL Lab Code1700. Reston, VA. doi:10.3133/tm10C19

Roberts, M.L., Burton, J.R., Elder, K.L., Longworth, B.E., McIntyre, C.P., von Reden, K.F., Han, B.X., Rosenheim, B.E., Jenkins, W.J., Galutschek, E., McNichol, A.P., 2010. A high-performance 14C accelerator mass spectrometry system. Radiocarbon 52, 228–235. doi:10.1017/S0033822200045252

Sarda, P., Graham, D., 1990. Mid-ocean ridge popping rocks: implications for degassing at ridge crests. Earth Planet. Sci. Lett. 97, 268–289. doi:10.1016/0012-821X(90)90047-2

Schwander, J., 1989. The transformation of snow to ice and the occlusion of gases, in: Oeschger, H., Langway, C.C. (Eds.), The Environmental Record in Glaciers and Ice Sheets. Wiley, New York, pp. 53–67.

Seltzer, Alan M., Ng, J., Danskin, W.R., Kulongoski, J.T., Gannon, R.S., Stute, M., Severinghaus, J.P., 2019a. Deglacial water-table decline in Southern California recorded by noble gas isotopes. Nat. Commun. 10. doi:10.1038/s41467-019-13693-2

Seltzer, A.M., Ng, J., Severinghaus, J.P., 2019. Precise determination of Ar, Kr and Xe isotopic fractionation due to diffusion and dissolution in fresh water. Earth Planet. Sci. Lett. 514. doi:10.1016/j.epsl.2019.03.008

Seltzer, Alan M., Ng, J., Severinghaus, J.P., 2019b. Precise determination of Ar, Kr and Xe isotopic fractionation due to diffusion and dissolution in fresh water. Earth Planet. Sci. Lett.

514, 156–165. doi:10.1016/j.epsl.2019.03.008

Seltzer, A.M., Severinghaus, J.P., Andraski, B.J., Stonestrom, D.A., 2017. Steady state fractionation of heavy noble gas isotopes in a deep unsaturated zone. Water Resour. Res. 53, 2716–2732. doi:10.1002/2016WR019655

Severinghaus, J.P., Bender, M.L., Keeling, R.F., Broecker, W.S., 1996. Fractionation of soil gases by diffusion of water vapor, gravitational settling, and thermal diffusion. Geochim. Cosmochim. Acta 60, 1005–1018. doi:10.1016/0016-7037(96)00011-7

Siade, A.J., Nishikawa, T., Rewis, D.L., Martin, P., Phillips, S.P., 2014. Antelope Valley-East Kern Water Agency, Palmdale Water District and Edwards Air Force Base Groundwater-Flow and Land-Subsidence Model of Antelope Valley, California, Scientific Investigations Report.

Solomon, D.K., 2000. 4He in Groundwater, in: Environmental Tracers in Subsurface Hydrology. Springer US, pp. 425–439. doi:10.1007/978-1-4615-4557-6_14

Solomon, D.K., Hunt, A., Poreda, R.J., 1996. Source of radiogenic helium 4 in shallow aquifers: Implications for dating young groundwater. Water Resour. Res. 32, 1805–1813. doi:10.1029/96WR00600

Stute, M., Forster, M., Frischkorn, H., Serejo, A., Clark, J.F., Schlosser, P., Broecker, W.S., Bonani, G., 1995. Cooling of Tropical Brazil (5C) During the Last Glacial Maximum. Science 269, 379–383. doi:10.1126/science.269.5222.379

Stute, M., Sonntag, C., Deák, J., Schlosser, P., 1992. Helium in deep circulating groundwater in the Great Hungarian Plain: Flow dynamics and crustal and mantle helium fluxes. Geochim. Cosmochim. Acta 56, 2051–2067. doi:10.1016/0016-7037(92)90329-H

Suckow, A., 2014. The age of groundwater - Definitions, models and why we do not need this

term. Appl. Geochemistry. doi:10.1016/j.apgeochem.2014.04.016

Tempest, K.E., Emerson, S., 2013. Kinetic isotopic fractionation of argon and neon during air-water gas transfer. Mar. Chem. 153, 39–47. doi:10.1016/j.marchem.2013.04.002

Torgersen, T., Clarke, W.B., 1985. Helium accumulation in groundwater, I: An evaluation of sources and the continental flux of crustal 4He in the Great Artesian Basin, Australia. Geochim. Cosmochim. Acta 49, 1211–1218. doi:10.1016/0016-7037(85)90011-0

Torgersen, T., Kennedy, B.M., Hiyagon, H., Chiou, K.Y., Reynolds, J.H., Clarke, W.B., 1989. Argon accumulation and the crustal degassing flux of 40Ar in the Great Artesian Basin, Australia. Earth Planet. Sci. Lett. 92, 43–56. doi:10.1016/0012-821X(89)90019-8

Tyroller, L., Brennwald, M.S., Busemann, H., Maden, C., Baur, H., Kipfer, R., 2018. Negligible fractionation of Kr and Xe isotopes by molecular diffusion in water. Earth Planet. Sci. Lett. 492, 73–78. doi:10.1016/J.EPSL.2018.03.047

Tyroller, L., Brennwald, M.S., Mächler, L., Livingstone, D.M., Kipfer, R., 2014. Fractionation of Ne and Ar isotopes by molecular diffusion in water. Geochim. Cosmochim. Acta 136, 60–66. doi:10.1016/j.gca.2014.03.040

Walsh, S.L., Demere, T.A., 1991. Age and Stratigraphy of the Sweetwater and Otay Formations, San Diego County, California 131–148.

Yan, Y., Bender, M.L., Brook, E.J., Clifford, H.M., Kemeny, P.C., Kurbatov, A. V., Mackay, S., Mayewski, P.A., Ng, J., Severinghaus, J.P., Higgins, J.A., 2019. Two-million-year-old snapshots of atmospheric gases from Antarctic ice. Nature 574, 663–666. doi:10.1038/s41586-019-1692-3

Yokochi, R., Sturchio, N.C., Purtschert, R., 2012. Determination of crustal fluid residence times using nucleogenic 39Ar. Geochim. Cosmochim. Acta 88, 19–26.

doi:10.1016/J.GCA.2012.04.034

Appendix A

We predict Δ^{40}Ar in groundwater by accounting for the release of radiogenic ^{40}Ar from weathering of old K-bearing aquifer minerals. In this idealized calculation, we first consider a single 1 cm^3 aquifer volume with bulk rock density ρ (g cm^{-3}), porosity φ, and fractional K abundance (by weight) F_K. The total K content (K_{tot}) within this 1 cm^3 volume is given (in mol) by:

$$K_{tot} = \rho\ (1\text{-}\varphi)\ F_K\ M^{-1} \quad \text{(A1)}$$

where M is the atomic weight of K. We then assume that some fraction (F_{old}) of the total K is sourced from extremely old minerals that have undergone substantial decay, while the remainder of the K is young and has experienced minimal radioactive decay. The initial ^{40}K content derived from old minerals ($^{40}K_0$) is given by:

$$^{40}K_0 = K_{tot}\ F_{old}\ F_{40K} \quad \text{(A2)}$$

where F_{40K} is the initial ^{40}K/K ratio. Next, we calculate the radiogenic ^{40}Ar content in this 1 cm^3 volume of aquifer rock ($^{40}Ar_{rock}$) based on the mean age τ of the old minerals (in Ma):

$$^{40}Ar_{rock} = {}^{40}K_0 \, \beta \, e^{-\lambda\tau} \quad (A3)$$

where λ is decay constant of ^{40}K (5.55×10^{-4} Ma^{-1}) and β is the branching of ^{40}K decay to ^{40}Ar versus ^{40}Ca (0.1048). We assume that some fraction ($F_{WEATHER}$) of aquifer rock is weathered by groundwater and quantitatively releases its ^{40}Ar, yielding an amount of dissolved radiogenic ^{40}Ar ($^{40}Ar_{rad\text{-}diss}$) given by:

$$^{40}Ar_{rad\text{-}diss} = {}^{40}Ar_{rock} \, F_{WEATHER} \quad (A4)$$

We determine the atmosphere-derived ^{40}Ar ($^{40}Ar_{atm\text{-}diss}$) dissolved in groundwater in the 1 cm^{-3} volume by assuming equilibrium with the atmosphere at a given temperature T, pressure P, and salinity S:

$$^{40}Ar_{atm\text{-}diss} = \rho \, s(T,S,P) \quad (A5)$$

where s is the solubility of ^{40}Ar in water in mol g^{-1}. Finally, we calculate $\Delta^{40}Ar$ as follows (in ‰):

$$\Delta^{40}Ar = {}^{40}Ar_{rad\text{-}diss}/{}^{40}Ar_{atm\text{-}diss} \quad (A6)$$

Declaration of interests

☒ The authors declare that they have no known competing financial interests or personal relationships that could have appeared to influence the work reported in this paper.

☐The authors declare the following financial interests/personal relationships which may be considered as potential competing interests: